Modeling Polymer Crystallisation Induced by a Moving Heat Sink

Sabin Adhikari,[a] Ahana Purushothaman,[b] Alejandro A. Krauskopf,[a] Christopher Durning,[a] Sanat K Kumar [a] and Sumesh P. Thampi,[*b]

Recent experimental work has shown that polymer crystallisation can be used to "move" and organize nanoparticles (NP). As a first effort at modeling this situation, we consider the classical Stefan problem but with the modification that polymer crystallisation does not occur at a single temperature. Rather, the rate of crystallisation is proportional to its subcooling, and here we employ a form inspired by the classical Avrami model to describe this functional form. Our results for the movement of the polymer crystallisation front, as defined as the point where the crystallinity is 50%, closely track the results of the classical Stefan problem. Thus, at this level of approximation, the crystallisation kinetics of the polymer do not cause qualitative changes to the physics of this situation. Inspired by this fact we study the more interesting situation where the directional recrystallisation of a polymer melt is considered, e.g., through the application of a moving heat sink over an initially molten polymer, reminiscent of a processing technique termed zone annealing. The polymer crystallisation shows that a steady state exists for a range of sink velocities. The solid-melt interface moves slightly ahead of the sink but at the same velocity. The steady-state distance between the sink and the interface decreases with increasing sink velocity - this is a consequence of the excess cooling provided by the sink over what is required to crystallise the melt. The most interesting new result is that the temperature of the crystal-melt interface decreases with increasing sink velocity. This is in line with the ansatz of Lovinger and Gryte[1] who suggested that larger zone annealing velocities correspond to progressively larger effective undercoolings at which polymer crystallisation occurs.

1 Introduction

Zone annealing (ZA), a technique which applies directional solidification for the purification of semiconductors,[2] has been explored as a potential processing technique for semicrystalline polymers[1,3,4] and block copolymers.[5–7] A relatively large body of theoretical work has been done in the metallurgical field focusing on the segregation of impurities during ZA of semiconductors.[8–11] This phenomenon, which is driven by the distribution coefficient for the impurity between the crystal and the liquid, can lead to ultrapure materials with relevance to electronics.

Our interest is towards obtaining a theoretical understanding of polymer zone annealing results first obtained by Lovinger and Gryte[1] nearly fifty years ago, and elaborated on by us recently[4]. In contrast to small molecules, e.g. silicon, polymers can be readily undercooled, and in fact there is a large body of literature that has quantified the rate of nucleation and crystal growth as a function of the degree of supercooling. Lovinger and Gryte conjectured that at steady state, the rate at which the polymer is moved through the temperature gradient sets the crystal growth velocity. Going further, they then argued that each such ZA protocol therefore corresponds to an isothermal crystallisation experiment at a temperature at which the crystal growth velocity matches the ZA velocity. While this conjecture is reasonable for understanding crystal growth rates, detailed experiments by us show that the structural features of the semicrystalline morphology (i.e., lamellar thickness, long period) also follow this conjecture. Thus, for example, the long period from a ZA experiment tracks that of an isothermal crystallisation experiment with the same growth rate. On the other hand, there are other features such as the orientation and shape of the spherulites which are quite different in the two cases - the ZA protocol results in spherulites that are elongated in the "flow" direction, while the isothermal experiments yield isotropic, spherical objects.

In this work, we report our first steps towards developing a theoretical framework to model the ZA of a polymer-like material whose growth kinetics are dependent on temperature (and also the extent of crystallinity). Initially, we will consider a one-dimensional polymer melt at its melting point and abruptly reduce the temperature at the origin to well below its melting point. We then track the temperature and fraction crystallised as a function of distance. Our results are found to closely parallel the results of the classical Stefan problem which concerns the growth of ice in polar seas and solves the evolution of the ice-water inter-

[a]*Department of Chemical Engineering, Columbia University, New York, New York 10027, United States; E-mail: sk2794@columbia.edu.*
[b] *Department of Chemical Engineering, Indian Institute of Technology, Madras, 600036, India; E-mail: sumesh@iitm.ac.in*

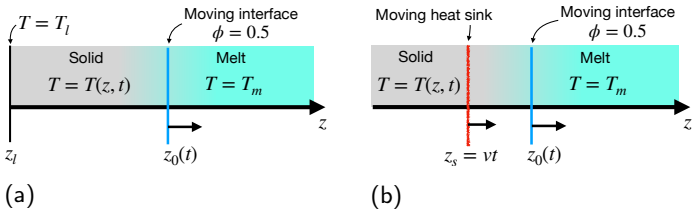

Fig. 1 Schematics representing solidification driven by a (a) stationary heat sink (b) moving heat sink.

face[12]. The spatial and temporal aspects of the evolution of temperature in this classical problem are not decoupled; instead, the temperature profile is a function of a similarity variable resulting from the spatial coordinate, time, and the thermal diffusivity. The progress of the solid-liquid interface is then proportional to the square root of the elapsed time (see Appendix A - B for in-depth discussion). In Stefan problem, melting occurs at a given temperature, the melting point, i.e., no supercooling is allowed. While our polymer model is able to crystallise under large supercoolings, we find the motion of the crystal-melt interface parallels the solution of the classical Stefan problem. This result then allows us to consider the behaviour of a polymer melt when a heat sink moves at constant velocity. We show that the polymer analog has a steady state for a range of sink velocities. Most interestingly, we find an inverse relationship between the velocity of the moving sink and the temperature of the solid-melt interface. This result verifies the experimentally inspired ansatz of Lovinger and Gryte, who showed that each steady state sink velocity corresponds to an equivalent isothermal crystallisation experiment.

This paper is organized as follows. In Section 2, we present the mathematical formulation of the directional phase change problem for polymers; in particular, we use the Avrami equation to model the crystallisation of polymers at large supercoolings. We then present the simulation details in Section 3, and modeling results for this formalism in Section 4, where we compare them to the traditional Stefan problem. In Section 5, we introduce a moving heat sink to the problem to resemble the ZA experiment. We conclude by relating the change in temperature at the interface to the velocity of the heat sink, and from there, we comment on the ansatz of Lovinger and Gryte. Separately, we present the numerical methods, a discussion of the classical Stefan problem, and our modeling results for the small molecule case in the Appendix A - B.

2 Mathematical formulation

We consider a polymer-like material whose growth kinetics are dependent on temperature and the extent of crystallinity. Let the material be in its melt state initially, and undergo the process of crystallisation under the action of an external driving force. In one dimension, the evolution of the temperature in the material is given by the unsteady heat equation,

$$\frac{\partial T}{\partial t} = \frac{k}{\rho C}\frac{\partial^2 T}{\partial z^2} + \frac{L}{C}\frac{\partial \phi}{\partial t} + Q, \tag{1}$$

which describes that the temporal change in temperature at any point in the material is due to three contributions: (i) the conductive heat flux from the surrounding regions, (ii) the extent of latent heat released during the crystallisation and (iii) the heat lost or gained due to the presence of any other heat sink or source. In Eqn 1, k is the thermal conductivity, ρ is the density and C is the specific heat capacity of the material. In general these properties will be different for the melt and solid phases. The latent heat associated with the phase change of the material is denoted by L and the heat input from an external source or sink is denoted by Q. If $\phi(z)$ represents the local volume fraction of the crystal phase, $\frac{\partial \phi}{\partial t}$ gives the rate of crystallisation at location z.

In this work, we use a modified form of the Avrami equation to model the crystallisation kinetics of the melt. In general the Avrami equation[13,14] describes the growth kinetics of crystallinity in a bulk material through the mathematical relation,

$$\phi(t) = 1 - \exp(-k_\phi t^n). \tag{2}$$

where k_ϕ and n are two constants associated with the growth kinetics. Eqn 2 assumes that the phase change is occurring at a constant temperature. In order to relax this assumption and hence to adapt Avrami kinetics into our model, we propose the following modifications.

Noting that, for an athermal case of interface reaction-controlled growth in one dimension, $n = 1$, Eqn 2 can be written in a differential form,

$$\frac{d\phi}{dt} = k_\phi(1-\phi). \tag{3}$$

to describe the local growth kinetics of the melt. However, Eqn 3 still prescribes the growth kinetics of an isothermal system and this assumption of constant temperature needs to be relaxed. This is imperative since the local temperature does not remain constant during the crystallisation process, and it is known that the rate of crystallisation increases with increased undercooling of the system. The exact temperature dependence that determines the crystallisation kinetics may be system dependent and might be complicated, but here we assume a simple linear relation between the rate of crystallisation and the degree of undercooling (the difference in temperature with respect to the melting point).

Thus, we may generalise Eqn 3 as

$$\frac{d\phi}{dt} = \begin{cases} R(1-\phi)\left(1-\frac{T}{T_m}\right), & T \leq T_m \\ 0, & T > T_m, \end{cases} \tag{4}$$

where T_m is a well-defined melting point for the material and R is a constant of proportionality. Thus, in contrast to the case of crystallisation of small molecules, which allows phase transition only at $T = T_m$, here the material is allowed to crystallise for a wide range of supercooling at any temperature below T_m. Also, Eqn 4 inherently assumes that the material has a maximum crystallinity of 1.

Hence, Eqn 1 and Eqn 4 describe the coupled evolution of the temperature and the crystallisation kinetics in the material: changes in temperature affect the kinetics of crystallisation locally while this change in growth kinetics changes the extent of latent heat released, thus affecting the local temperature profile. Having described this process mathematically, we will consider the following two cases in this work.

Case I - Crystallisation due to a stationary heat sink: Consider that the melt be at a uniform temperature $T \geq T_m$ initially. At $t = 0$, a constant temperature $T_l < T_m$ is applied at $z = z_l$, the left boundary of the material. Consequently the system cools down and the melt crystallises into a solid phase. This scenario is depicted in Fig. 1a and resembles the classical Stefan problem (see Appendix A for the description of the Stefan problem). To simplify the analysis, the following non-dimensional variables are introduced: $\tilde{T} = \frac{T-T_m}{T_m-T_l}$, $\tilde{\phi} = \phi$, $\tilde{t} = R\frac{T_m-T_l}{T_m}t$ and $\tilde{z} = \frac{z}{d}$ where $d = \sqrt{\frac{k}{R\rho C\frac{T_m-T_l}{T_m}}}$ is an appropriate length scale arising from the thermal diffusivity, $k/(\rho C)$, and the rate of crystallisation, R. The rescaled temperature, $\tilde{T}$, is zero at the melting point and -1 at the left boundary ($z = z_l$). Therefore, Eqn 1 and Eqn 4 may be rewritten in a non-dimensional form,

$$\frac{\partial \tilde{T}}{\partial \tilde{t}} = \frac{\partial^2 \tilde{T}}{\partial \tilde{z}^2} + \lambda \frac{\partial \tilde{\phi}}{\partial \tilde{t}}, \tag{5}$$

and

$$\frac{d\tilde{\phi}}{d\tilde{t}} = \begin{cases} -(1-\tilde{\phi})\tilde{T}, & \tilde{T} \leq 0 \\ 0, & \tilde{T} > 0, \end{cases} \tag{6}$$

where we have taken $Q = 0$ and introduced a non-dimensional parameter $\lambda = \frac{L}{C(T_m-T_l)}$. This parameter λ is the ratio of the temperature scale set by the latent and specific heat capacity of the material, L/C, to the imposed driving force for crystallisation $T_m - T_l$. With the above non-dimensionalisation, λ turns out to be the only parameter that governs the transport processes considered here.

Case II - Crystallisation with a moving heat sink: As earlier, consider the material to be initially at a uniform temperature $T(z,t=0) \geq T_m$. A heat sink is then initialised at the left boundary $z = z_l$ at $t = 0$ that moves in the positive z direction with a velocity v. Consequently, as in the previous case, the melt crystallises - this scenario is depicted in Fig. 1b. In this problem, the heat sink can be modelled in two different ways:

1. A 'constant temperature sink' - when it is brought in contact with the sample, it rapidly cools down the contact region of the sample and renders this region a temperature T_l. Mathematically, the heat sink can be incorporated into the formulation by imposing the constraint,

$$T(z,t) = T_l, \quad \text{for} \quad z = vt. \tag{7}$$

2. A 'constant heat flux sink' - when it is brought in contact with the sample, it absorbs heat energy from the sample at a constant rate. Mathematically, this heat sink can be modelled as a delta function of strength $\dot{q}$ in Eqn 1,

$$Q = -\frac{\dot{q}}{\rho C}\delta(z - vt). \tag{8}$$

In the discussion that follows we take the former approach. A comparison between the two approaches is provided in Appendix B.4, where we describe a similar scenario, the solidification of simple fluids.

The stationary heat sink in Case I and the moving heat sink in Case II take away the latent heat released during the crystallisation of the solid as well as the specific heat required to bring down the temperature in the material. Thus as the melt continues to crystallise, the resulting solid-melt interface progressively moves in the z-direction as shown in Fig. 1. The temperature and crystallinity profiles in the material evolve in time. Our goal is to find the temperature and crystallinity profiles throughout the material at all times, as well as to track the location of the solid-melt interface in relation to the heat sink position in both cases.

3 Simulation details

The two cases mentioned above, namely the crystallisation with a stationary and a moving heat sink, are analyzed by solving Eqn 5 and Eqn 6 along with the constraint that describes the heat sink. For this purpose, consider the 1-D computational domain from $z = z_l$ to $z = z_r$. At any given time t, the heat sink is located at $z = z_l$ for Case I and $z = z_s$ for Case II in the solid phase. The entire domain is discretised into a grid with a spacing of Δz and hence the temperature and the degree of crystallinity take discrete values. The right boundary of the domain, $z = z_r$ is assumed to be insulated.

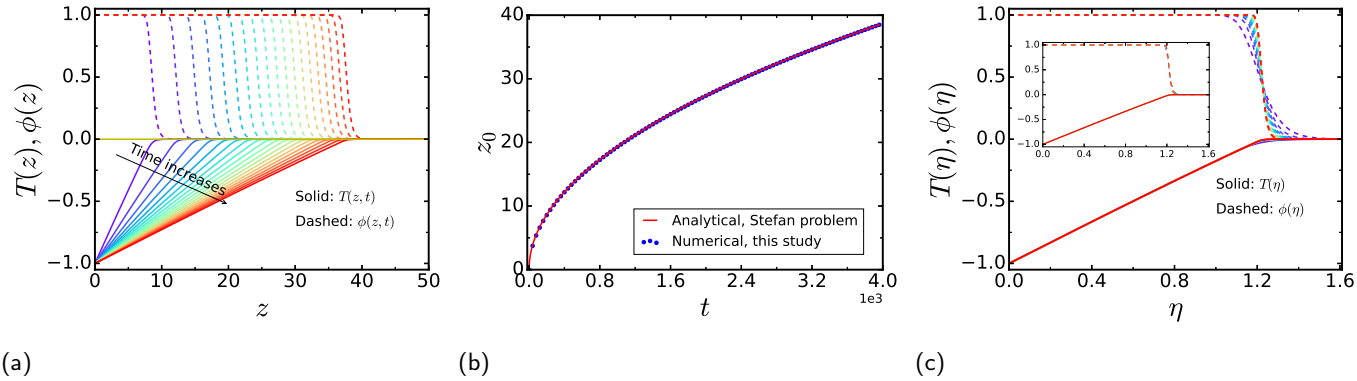

Fig. 2 Case I: (a) Evolution of temperature (T) and crystal volume fraction (ϕ) with time (t) during the crystallisation of a polymer melt induced by a stationary heat sink. Continuous lines are temperature vs position, $T(z)$ while the dashed curves are corresponding $\phi(z)$ profiles. Different curves correspond to different instances in time separated by equal time intervals (of 200 time units). At $t = 0$, temperature is a step function, $T = -1$ at $z = 0$ and $T = 0$ everywhere else. But ϕ has a uniform profile, with $\phi = 0$ at all z at $t = 0$. (b) The position of solid–liquid interface (z_0), as defined by the position where $\phi = 0.5$, vs time t from numerical simulations is compared to the analytical expression from the corresponding Stefan problem of a simple, low molecular weight material. The position of the interface in the Stefan problem is given by $z_0 = 2a\sqrt{t}$ where $a = 0.306$ for $\lambda = 5$. (see appendix B.1) (c) Self similar profiles of temperature and crystallinity, in the similarity variable $\eta = z/\sqrt{t}$. The inset shows self similar profiles of both T and ϕ when the first ten profiles are removed, i.e., profiles only after $t = 2000$ are shown.

The evolution of the temperature is calculated by the method of lines, wherein the spatial derivative on the right hand side of the heat balance, Eqn 5, is approximated using a second-order accurate central difference scheme (see Eqn 14), and the resulting ordinary differential equations are simultaneously integrated along with Eqn 6. The numerical technique employed for computation is a fourth-order Runge–Kutta integration algorithm. In Case II, the temperature due to the heat sink described by Eqn 7 is taken as a square well profile of width $= 2\Delta z$. During the integration, this heat sink is moved with a constant velocity v so that z_s is updated at every time step as $z_s = vt$. The results are presented in Section 4 for the case of a stationary heat sink and in Section 5 for the case of a moving heat sink.

For the simulations we have considered the material properties of poly(ethylene oxide) (PEO), the polymer employed by Lovinger and Gryte[1] as well as in our follow-up investigation[4]. The material is considered as homogeneous with well-defined, temperature- and crystallinity-independent material properties. The typical material parameters are: melting point $T_m = 352.15$ K, specific heat capacity $C = 1.853$ Jg^{-1}K^{-1}, and latent heat $L = 205$ Jg^{-1}. Since typical crystallisation temperatures for PEO are $323 - 333$ K, the value of λ ranges from 3.81 to 5.82. For a representative value, we use $\lambda = 5$ for all of our numerical computations.

For comparison, similar results for the crystallisation of a simple fluid made up of small molecules using a stationary and a moving heat sink are given in Appendix B. In that scenario, the numerical results are further justified using an analytical solution.

4 Case I: Crystallisation of polymer melt induced by a stationary heat sink

In this case, the material is assumed to be initially at its melting point T_m with zero crystallinity everywhere. At $t = 0$, the temperature on the left boundary is reduced to T_l. Then, heat flows from right to left, the melt starts crystallising, and the solid-melt interface moves to the right. Fig. 2 shows the results obtained from the simulations. Now onwards, all the physical quantities in the plots are in dimensionless units, but we drop the tilde sign for simplicity of presentation. Also, note that our mathematical formulation in the previous section does not require the material to be initially at its melting point, but here, we set the initial temperature everywhere to be T_m for simplicity.

Fig. 2a shows the evolution of temperature T, and crystal volume fraction ϕ, with time t. The continuous curves correspond to temperature vs. position (z), while the dashed curves are the corresponding z-dependent ϕ profiles at different times. The initial temperature profile is a step function, and the initial crystal volume fraction is uniformly 0 everywhere. The heat is lost to the stationary sink, and the temperature in the material decreases with time. Thus, at any time the temperature varies from $T = -1$ at $z = 0$ to $T = 0$ for $z > 0$ in the domain. As time proceeds, the region over which the temperature is not the same as the initial temperature ($T \neq T_m$) expands. This change in the temperature profile is fast at the beginning, but it slows down with time, as evident from the crowding of the temperature pro-

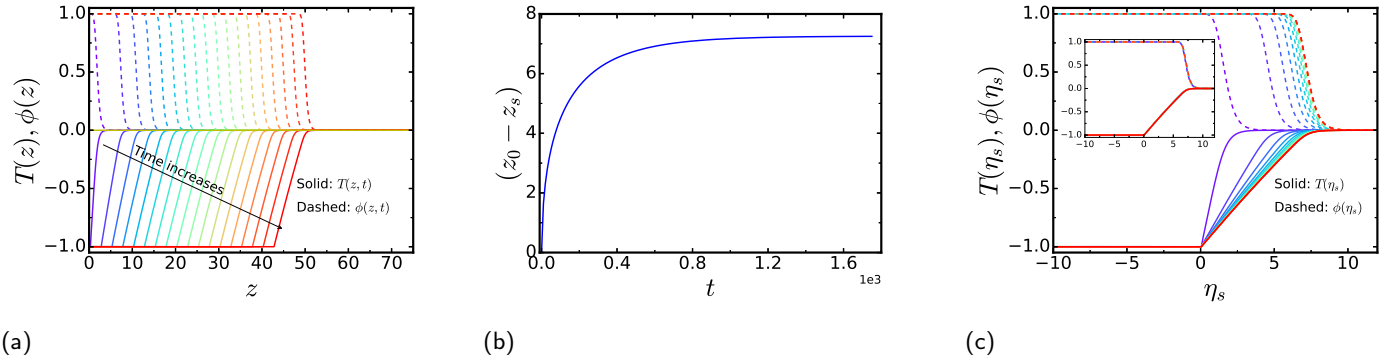

(a) (b) (c)

Fig. 3 Case II: (a) Temperature (T) and crystallinity (ϕ) profiles at different times when a heat sink of constant temperature -1 moving with a velocity $v = 0.025$ is introduced in the melt. The two ends of the one dimensional domain are thermally insulated and the sink moves from left to right starting from $z = 0$ at $t = 0$. The location of the heat sink in this figure can be tracked by analyzing the temperature profiles, i.e at the point where the temperature starts to rise from -1. (b) Relative position of the solid-melt interface w.r.t. the location of the heat sink ($z_0 - z_s$) versus time (t). (c) The temperature and the crystallinity profiles in the co-moving frame, i.e, $T(\eta_s)$ and $\phi(\eta_s)$ where $\eta_s = z - vt$. The inset shows the same profiles but only at later times, $t > 1000$ showing a collapse of the data at all times, of both temperature and crystallinity profiles.

files at later times. The cooling of the material leads to the solidification of the melt, and thus the crystal volume fraction in the solid, ϕ, increases with time. However, ϕ is not uniform in the solid phase. Instead, at any time t, the volume fraction of crystals continuously changes from its maximum value of 1 to its minimum value 0, thus exhibiting a spatially dependent value. The profiles of ϕ resemble a hyperbolic tangent function, which shows that most of the variation in ϕ is restricted to a smaller region in z. As time proceeds, the crystallinity continues to develop.

It may be noted that both the ϕ and T curves are very flat near $T = 0$ and $\phi = 0$ (i.e, in the neighbourhood of the solid-melt interface), but that the T curve "trails" the corresponding ϕ curve. We conjecture that since the crystallisation of the polymer generates heat, this causes the temperature profiles to trail the crystallisation profiles. Consistent with this notion, we find that the offset between the T and ϕ profiles decreases with decreasing λ.

Since the interface that separates the solid and the liquid phases is not sharp, but rather diffuse over a region, we define the following measure. We designate $z = z_0$ where $\phi = 0.5$, and define this as the location of the solid-melt interface. We monitor the progress of z_0 as a function of time. Fig. 2b shows the interface location of $z_0(t)$ as crystallisation proceeds to the right. It is evident that z_0 increases with time, quite quickly in the beginning while slowing down as time proceeds.

Further, this result describing the translating interface obtained from the numerical simulations is compared to the analytical solution from the corresponding Stefan problem. As explained in Appendix A, the solution to the Stefan problem dictates that the position of the solid-melt interface during the soldification induced by a stationary heat sink should follow a diffusive behaviour, $z_0 = 2a\sqrt{t}$, where a is to be determined by solving the transcendental equation $a\exp(a^2)\mathrm{erf}(a) = \frac{1}{\lambda\sqrt{\pi}}$. Fig. 2b shows that our numerical result for $z_0(t)$ tracks the analytical solution obtained from the Stefan problem very well. This is interesting, since our model incorporates the Avrami kinetics of crystallisation, unlike the classical Stefan problem, which describes the phase change of a simple material exhibiting a well-defined melting point. This close match between the two cases demonstrates the generality of the Stefan solution: that even a polymer melt which follows Avrami kinetics obeys the classical square root growth of the solid-melt interface position during the solidification of the material.

This similarity in the growth kinetics between the two problems, namely the standard Stefan problem and the crystallisation of a polymer melt, is also reflected in the temperature and crystallinity profiles. In other words, both the temperature and crystallinity profiles conform to a self-similar solution, a characteristic of the solution of the Stefan problem. This is shown in Fig. 2c, where both temperature and crystallinity are plotted as a function of the self-similar variable $\eta = z/\sqrt{t}$. Clearly, the data presented in Fig. 2a shows a collapse with η. The slight variations observed in the collapse can be attributed to some transients in the problem, as the inset which shows the profiles only at later times ($t \geq 2000$) shows no variations, indicating a perfect collapse of $T(z,t)$ to $T(\eta)$ and $\phi(z,t)$ to $\phi(\eta)$.

Thus, the system of a crystallising melt reaches a self-consistent solution where the latent heat released during crystallisation of the melt, as well as the specific heat required for reducing the temperature in the solid phase, are

taken away by the stationary heat sink located at the boundary. This heat balance determines the velocity of the solid-melt interface as $\propto 1/\sqrt{t}$. The interface continuously moves away from the sink with an ever-decreasing velocity, and without reaching a steady state. This is characteristic of a growth problem which has no inherent length, time or velocity scales. In the discussion below, we show how this unsteady solution changes by the presence of a moving heat sink.

5 Case II: Crystallisation of polymer melt induced by a moving heat sink

Now, we consider the second case, where a polymer melt at temperature $T = T_m$ is cooled by a moving heat sink. The initial temperature is uniform everywhere, and let the two boundaries of the domain be thermally insulated. At $t = 0$, we introduce a heat sink at the left boundary, and the heat sink moves from left to right at a constant velocity v. This scenario is depicted in Fig. 1b. As the sink removes heat, the temperature of the melt is lowered such that the polymer begins to crystallise. Note that, in line with the tendency of polymers to solidify in a wide range of supercoolings, we allow the material to crystallise at any temperature below T_m, in contrast to the small-molecule case, which only allows crystallisation at $T = T_m$.

As before, we track both the temperature and crystallinity profiles, as shown in Fig. 3a. The temperature shows a piecewise profile with temperature remaining constant ($T = -1$) over a range of z, then increasing and following an exponential-like profile, and finally again adopting a constant value ($T = 0$), which happens in the melt phase. The location of the first kink in the profile, where temperature changes from a constant to the exponential-like profile, represents the location of the moving heat sink. To the left of the heat sink, the temperature is constant, and is equal to the temperature of the moving heat sink. Temperature is varying only in the region sandwiched between the instantaneous location of the heat sink and the melt phase. This is in contrast with the previous case, where the temperature in the entire solid phase was changing since the heat sink was stationary. The cooling of the material also results in the development of the crystallinity; however, this is similar to the previous case where $\phi = 1$ in most of the domain, and it sharply changes to 0 in the melt phase. Again, the temperature profiles "trail" the crystallinity profiles due to the latent heat released during the crystallisation process.

The temperature and crystallinity profiles shown in Fig. 3a are at equal time intervals. It is evident from the figure that the "distance" between the equally time spaced profiles initially decreases, but becomes a constant afterwards. This suggests that the system is in a transient state in the initial part, during which the extent of cooling slows down with time, but at later times, the system reaches a steady state. In fact, on monitoring the slopes of the temperature profiles at the location of the heat sink, it becomes clear that the slopes decrease with time and eventually reach a constant, indicating that the rate of flow of heat from the sample to the heat sink decreases as time progresses before reaching a steady state. This result is in contrast to the ever changing profiles obtained in the previous case, in Fig. 2a, where both the temperature and crystallinity profiles showed a spatio-temporal dependence of the form $T(z/\sqrt{t})$ and $\phi(z/\sqrt{t})$. Observation of attainment of a steady state is verified by calculating $z_0 - z_s$, the difference between the position of the solid-melt interface and the heat sink, and is shown in Fig. 3b. Again, note that we define the solid-melt interface to be where $\phi = 0.5$. Fig. 3b shows that, initially, the system is in a transient state, as the difference between the interface and sink location increases with time. After a certain time, however, the distance between the interface and the sink reaches a plateau, indicating that the system has achieved a steady state.

Since temperature is still a function of both z and t even when the crystallisation is proceeding in a steady state fashion, we introduce a new variable, $\eta_s = z - vt$. This is equivalent to moving to a coordinate system which is translating along with the heat sink. In this co-moving frame, η_s measures the distance from the heat sink and, therefore, $\eta_s = 0$ corresponds to the location of the heat sink. The temperature and crystallinity profiles presented in Fig. 3a are replotted in Fig. 3c as a function of η_s. The inset shows the same data set but only plotted for later times. Clearly, the figure illustrates that, after an initial transient evolution, the system reaches a steady state, with both temperature and crystallinity profiles being a function of only η_s, the distance from the heat sink.

The reason for the initial transients can be understood as follows. It is obvious that there are two velocity scales in the problem: an imposed velocity v and an inherent velocity $\sqrt{(k/\rho C)/t}$. At very short times ($t \to 0$) we have $v << \sqrt{(k/\rho C)/t}$, i.e, the imposed velocity is much smaller than the inherent (diffusive) velocity of the interface. Then, the system behaves as in Case I, as cooling and crystallisation of the melt are faster, and the position of the solid-melt interface grows with large velocity. However, the growth velocity decreases with time, and as time proceeds, it approaches the velocity of the moving sink (inherent velocity is comparable to the imposed velocity). Then, the system is no longer similar to Case I, but rather, the kinetics are driven by the moving heat sink, and the temperature profiles switch over to the piecewise profiles as shown in Fig. 3a .Comparing the imposed and the inherent velocity scales, it

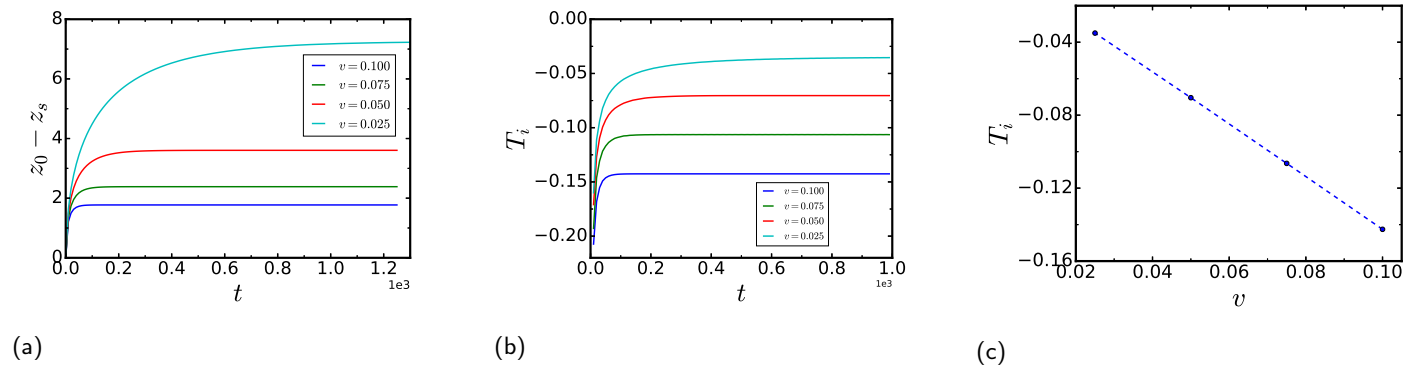

(a) (b) (c)

Fig. 4 (a) Relative position of the interface w.r.t. the sink ($z_0 - z_s$) and (b) interface temperature (T_i) as a function of time (t) for different sink velocities (v). Plots (a) and (b) show the existence of steady states. (c) Solid–liquid interface temperature (T_i) as a function of sink velocity (v).

may be deduced that the transition from a self-similar to the steady-state solution will occur at $t \sim (k/\rho C)/v^2$.

Appendix B.4 shows that the attainment of a steady state crystallisation of the melt by a moving heat sink is much more generic, and is independent of (i) the nature of the heat sink, namely whether the heat sink imposes a constant temperature or it drains the heat energy at a constant rate, and (ii) the nature of boundary conditions imposed on the domain boundaries, namely whether it is a constant temperature (Dirichlet boundary condition) or a constant heat flux (Neumann boundary condition). These calculations, done for the case of crystallisation of small molecules (see Fig. 5), also reveal the universal features of the temperature profiles due to a moving heat sink: the temperature profiles are piecewise with three distinct regions - (i) the temperature to the left of the heat sink is a constant (for $z < z_s$), (ii) the temperature of the sandwiched layer between the heat sink and the solid-melt interface varies exponentially (in $z_s < z < z_0$), and (iii) the melt phase continues to be at its melting point (for $z > z_0$).

The temperature profile corresponding to a steadily moving crystallising front is clearly different from the similarity profile described by the similarity variable $\eta = z/\sqrt{t}$, a characteristic feature of the classical Stefan problem in Case I. This difference may be understood as follows: as noted above, Case I lacks inherent length, time, or velocity scales to describe the growth of the solid-melt interface. Mathematically, the absence of these inherent scales results in a similarity profile of the temperature in the solid phase. Driving the system with a steadily moving heat sink imposes a velocity (velocity of the heat sink) and thus a length scale (the separation distance between the heat sink and the solid-melt interface). Consequently, the system no longer displays the self-similar profile for temperature, but rather achieves a steady-state with the temperature profile as only a function of η_s, the distance from the heat sink. When the imposed velocity approaches zero, the system regains the self-similar profile.

Similar results are found for different velocities of the heat sink ($v = 0.025, 0.050, 0.075, 0.100$) as shown in Fig. 4a. Here, the position of the interface relative to the moving sink is plotted as a function of time. Clearly, the system reaches a steady state, with the solid-melt interface and the location of the heat sink attaining a constant separation in all cases. As discussed earlier, the time at which the system reaches steady state depends on the velocity of the heat sink. It can be seen that the transition time increases with a decrease in v (more precisely as $\sim 1/v^2$). Moreover, it may be noted that the steady-state separation distance between the heat sink and the solid-melt interface increases with a decrease in the velocity of the sink. This may be expected, as a faster moving heat sink can approach the solid-melt interface more easily.

Similarly, Fig. 4b shows the temperature of the interface as a function of time for these four sink velocities. Note that this interface temperature T_i is defined as the temperature at which $\phi = 0.5$, in accordance to the definition of z_0. Again, the figure demonstrates that the directional polymer crystallisation process under a moving heat sink reaches a steady state for the range of velocities explored here. Moreover, it can be seen that the interface temperature decreases with an increase in the velocity of the heat sink. This happens because a faster moving heat sink can access a larger volume of the crystallising material, and thus the heat sink can less efficiently drain the heat from the melt. This results in T_i decreasing with an increase in the sink velocity. Analytical and numerical calculations described in the appendix for the case of small molecules justify this argument; there, it is shown in Fig. 8 that the temperature of the solid phase decreases with increasing velocity of the heat sink and with

decreasing strength (heat flux) of the heat sink. This dependence of the interface temperature on the sink velocity is plotted in Fig. 4c. This plot brings us back to the main motivation for the present study: Fig. 4c supports the ansatz of Lovinger and Gryte [1] that there exists an equivalent isothermal crystallisation temperature for each ZA velocity, and that this temperature decreases with increasing ZA velocity. These results also validate our experimental results,[4] namely that the long period of a ZA polymer tracks the long period of an isothermally crystallised polymer, when the ZA velocity is converted to an effective isothermal crystallisation temperature through the Lauritzen-Hoffman crystal growth theory.

6 Conclusions

We develop a theoretical framework to model polymer crystallisation when induced by a moving heat sink, a feature that uniquely characterises the ZA process. We introduce a mathematical formulation wherein the Avrami formalism for crystallisation of polymers is incorporated into the standard heat transfer equation. Simulations are carried out for two cases, namely the case where the heat sink is stationary and the case where the heat sink is allowed to move at a constant velocity. Similarities between the stationary heat sink problem and the traditional Stefan problem are demonstrated through these simulations, as it is observed that both the temperature and crystallinity profiles exhibit a self-similar form. In contrast, we find that a steady state is achieved upon introducing a moving heat sink, and that the interface temperature decreases as the velocity of the heat sink is increased. These results, in combination, verify the ansatz of Lovinger and Gryte, who conjectured that there exists an effective isothermal crystallisation temperature for each ZA velocity. Evidently, the polymer crystallisation problem tracks the results of the Stefan problem except for this last aspect which critically distinguishes between these two different situations.

At high undercooling, when crystal growth is controlled by slow mass transport, the use of the Avrami equation to model local growth of crystallinity might yield poor results. In this context, alternate approaches such as phase field models[15–19] may be useful. Typically, phase field models assume a local free energy density and the resulting equation of motion for the local order parameter is a nonlinear differential equation. The nonlinearity may be inherent in the free energy term or it may appear in an order parameter dependent diffusivity or in coupling with hydrodynamics. Compared to using our simple linear equation for the growth of local crystallinity, starting from such a more general, nonlinear equation would provide more accurate results, particularly at high undercooling. Nevertheless, the current model provides important insights on the evolution of the growth front and the existence of a steady state when crystallisation is driven by a moving sink and it can be easily improved by replacing the Avrami equation for crystal growth by a more general nonlinear relation.

7 Conflicts of interest

The authors declare no competing financial interests.

8 Acknowledgments

This work was supported by grants DE-SC0018182, DE-SC0018135, and DE-SC0018111, funded by the U.S. Department of Energy, Office of Science. A.A.K. acknowledges funding from the Gates Millennium Scholars program under Grant No. OPP1202023 from the Bill & Melinda Gates Foundation.

References

1 A. J. Lovinger and C. C. Gryte, *Macromolecules*, 1976, **9**, 247–253.

2 W. Pfann, *Science*, 1962, **135**, 1101–1109.

3 C. Ye, L. Zhang, G. Fu, A. Karim, T. Kyu, A. L. Briseno and B. D. Vogt, *ACS applied materials & interfaces*, 2015, **7**, 23008–23014.

4 A. A. Krauskopf, A. M. Jimenez, E. A. Lewis, B. D. Vogt, A. J. Müller and S. K. Kumar, *ACS Macro Letters*, 2020, **9**, 1007–1012.

5 P. W. Majewski and K. G. Yager, *ACS Nano*, 2015, **9**, 3896–3906.

6 S. Samant, J. Strzalka, K. G. Yager, K. Kisslinger, D. Grolman, M. Basutkar, N. Salunke, G. Singh, B. Berry and A. Karim, *Macromolecules*, 2016, **49**, 8633–8642.

7 G. Singh, K. G. Yager, D.-M. Smilgies, M. M. Kulkarni, D. G. Bucknall and A. Karim, *Macromolecules*, 2012, **45**, 7107–7117.

8 W. Tiller, K. Jackson, J. Rutter and B. Chalmers, *Acta Metallurgica*, 1953, **1**, 428–437.

9 H. Reiss, *JOM*, 1954, **6**, 1053–1059.

10 L. Burris, C. Stockman and I. Dillon, *JOM*, 1955, **7**, 1017–1023.

11 I. Braun and S. Marshall, *British Journal of Applied Physics*, 1957, **8**, 157.

12 J. Stefan, *Annalen der Physik*, 1891, **278**, 269–286.

13 M. Avrami, *The Journal of chemical physics*, 1939, **7**, 1103–1112.

14 M. Avrami, *The Journal of chemical physics*, 1940, **8**, 212–224.

15 H. Löwen, J. Bechhoefer and L. S. Tuckerman, *Physical Review A*, 1992, **45**, 2399.

16 J. F. Douglas, K. Efimenko, D. A. Fischer, F. R. Phelan and J. Genzer, *Proceedings of the National Academy of Sciences*, 2007, **104**, 10324–10329.

17 L. Gránásy, T. Pusztai and J. Douglas, *Encyclopedia of polymers and composites. Springer, Berlin*, 2013, 1–35.

18 G. Tegze, L. Gránásy, G. I. Tóth, J. F. Douglas and T. Pusztai, *Soft Matter*, 2011, **7**, 1789–1799.

19 R. Mehta and T. Kyu, *Journal of Polymer Science Part B: Polymer Physics*, 2004, **42**, 2892–2899.

20 H. Weber, *Die partiellen differential-gleichungen der mathematischen physik: bd. Hülfsmittel aus der theorie der linearen differentialgleichungen. Wärmeleitung. Elasticitäts-theorie. Elektrische schwingungen. Hydrodynamik*, F. Vieweg und Sohn, 1901, vol. 2.

21 L. Rubinšteĭn, *The Stefan Problem*, American Mathematical Society, 2000, vol. 8.

22 C. Hsieh, *International Journal of Heat and Mass transfer*, 1995, **38**, 71–79.

23 M. Zerroukat and C. R. Chatwin, *Computational Moving Boundary Problems*, Research Studies Press, 1994, vol. 8.

Appendix

In the appendix we describe the case I and case II introduced in the manuscript but for the case of small molecules. Thus, the material under consideration shows a sharp melting point and ϕ is a step function changing abruptly from $\phi = 1$ in the solid phase to $\phi = 0$ in the melt phase. We make predictions for this class of systems and present results, especially the excellent agreement between the analytical theory and the simulations.

A Case I - Stefan problem

Neumann developed the first known analytical solution to the directional phase change problem in the 1860s,[20] though Josef Stefan's later work on ice formation is better known.[12] In the classical case, the system modeled is a block of solid at some temperature below its equilibrium melting point. At time t=0, the temperature at the origin, z=0, is raised above the melting point. The analytical solution of this problem can be obtained through the use of standard unsteady state heat balance equations, with the interesting feature that they hinge on tracking the interface boundary (i.e., the location of the liquid-solid interface) with what is known as the Stefan boundary condition. This prescribes that the velocity of the interface is set by a heat balance, namely the latent heat of phase change is balanced by the heat conducted in/out at the interface. Mathematically, and for a liquid-solid interface, this heat balance is,

$$k_s \left.\frac{\partial T}{\partial z}\right|_{solid} - k_l \left.\frac{\partial T}{\partial z}\right|_{liquid} = \rho L \frac{dz_o}{dt} \tag{9}$$

where k_s and k_l are the thermal conductivity of the solid and liquid, respectively, T is the temperature, z is the spatial coordinate normal to the interface, L is the latent heat of melting, ρ is the mass density, dz_0/dt is the velocity of the interface and z_0 is the interface location. Then, eqn 4 is irrelevant and the evolution of the transient temperature profile can be determined analytically using the standard solution techniques of partial differential equations and subjecting the solution to the following initial and boundary conditions: $T(z = z_l, t) = T_l$ and $T(z, t = 0) = T_m$. In addition, the solution must satisfy the Stefan boundary condition (eqn 9). The obtained temperature profile at any time is[21]

$$T(z,t) = \begin{cases} T_l + \frac{(T_m - T_l)}{\mathrm{erf}(a)} \mathrm{erf}\left(\frac{z - z_l}{\sqrt{4\alpha t}}\right) & \text{for} \quad z_l \le z \le z_0 \\ T_m & \text{for} \quad z > z_0 \end{cases} \tag{10}$$

where erf stands for the error function. The position of the interface at any time is given by $z_0(t) - z_l = a\sqrt{4\alpha t}$. The constant a is determined by the transcendental equation $a \exp(a^2) \mathrm{erf}(a) = \frac{C(T_l - T_m)}{L\sqrt{\pi}}$.

From eqn 10 it is clear that the Stefan problem does not have a steady-state solution. The melting of the solid continues infinitely with the melting front diffusively progressing ($z_0 \propto \sqrt{t}$) away from the left boundary ($z = z_l$). The temperature in the liquid region continuously evolves in space and time, but the spatio-temporal evolution of temperature follows a universal curve in terms of the similarity variable $\eta = (z - z_l)/\sqrt{t}$. In other words, the temperature profiles in the liquid at all times can be collapsed onto a single curve $T(\eta)$.

B Case II: Stefan problem when driven by a moving heat sink

B.1 Analytical solution for the steady state

Consider eqn 8 given in the reference frame moving with the sink,

$$\frac{\partial T}{\partial t} = \frac{k}{\rho C} \frac{\partial^2 T}{\partial z^2} + v \frac{\partial T}{\partial z} \quad \text{when} \quad z \neq z_s. \tag{11}$$

We propose a piecewise solution to this problem

$$T = T_c = T_m + \frac{1}{C}\left[\frac{\dot{q}}{\rho v} - L\right] \quad \text{for } z < z_s \tag{12a}$$

$$T = T_m - \frac{L}{C} + \frac{L}{C}\exp\left(\frac{z_0 - z}{\kappa}\right) \quad \text{for } z_s < z < z_0 \tag{12b}$$

We can obtain the separation distance between the heat sink and the solid-melt interface at steady state as,

$$z_0 - z_s = \frac{k}{\rho C v}\ln\frac{\dot{q}}{\rho v L} \tag{13}$$

This expression shows the manner in which the system attains a self-consistent steady-state solution. If we impose a heat sink moving with a velocity v, then the system is constrained to have a characteristic velocity scale v and a characteristic length scale $z_0 - z_s \propto -1/v \times \ln(v)$ which is the steady state separation distance between the heat sink and the solid-melt interface. While this analytical solution is consistent with the predictions of Hsieh[22] we verify the existence of steady state solutions and the conditions leading to it by solving the unsteady heat equation numerically.

B.2 Numerical method for solving a sharp interface problem

Consider the 1-D computational domain from $z = z_l$ to $z = z_r$. The entire domain is discretised into a grid with a spacing of Δz and hence the temperature takes discrete values T_i. Here the subscript i stands for the ith grid point. Let i_b be the grid point located at a distance $p\Delta z$ in the melt phase just next to the phase boundary. The evolution of the temperature is calculated by conveniently dividing the domain into three regions and adopting different strategies in each region:

1. Region 1 ($0 \le i < i_b$): In this case, the spatial derivative on the right hand side of the heat balance is approximated using a second-order accurate central difference scheme to obtain

$$\frac{dT_i}{dt} = \frac{k}{\rho C}\left[\frac{T_{i+1}(t) + T_{i-1}(t) - 2T_i(t)}{(\Delta z)^2}\right] \tag{14}$$

   i_b ordinary differential equations (i.e, $0 \le i < i_b$) in time.

2. Region 2 ($i = i_b$): In order to account for the heat transfer process at the melting boundary through (i) the Stefan boundary condition (eqn 9) and (ii) the continuity of temperature, $T = T_m$ at $z = z_0$, the following procedure is adopted[23]. The temperature profile in the vicinity of the two phase boundary is approximated with a quadratic polynomial which is obtained from a three-point Lagrange interpolation method. Then the evolution of temperature at $i = i_b$ is obtained as

$$\frac{dT_{i_b}}{dt} = \frac{2k}{\rho C(\Delta z)^2}\left[\frac{T_{i_b-1}(t)}{p+1} - \frac{T_{i_b}(t)}{p} + \frac{T_m}{p(p+1)}\right]. \tag{15}$$

   In this way, $T = T_m$ at $z = z_0$ is explicitly imposed in the computations. However, $p = (z_0 - i_b\Delta z)/(\Delta z)$, which describes the location of the phase boundary between the grid points i_b and $i_b + 1$, is an unknown and to be determined. This is done by rewriting the Stefan boundary condition (eqn 9) as

$$\frac{dp}{dt} = -\frac{k}{L\rho(\Delta z)^2}\left[\frac{pT_{i_b-1}}{p+1} - \frac{pT_{i_b}}{p+1} + \frac{(2p+1)(T_m - T_{i_b})}{p(p+1)}\right] \tag{16}$$

3. Region 3 ($i > i_b$): This region represents the uncrystallised melt and therefore it is assumed that the temperature $T_i = Tm$ for $i > i_b$.

The temperature in all three regions are to be simultaneously evolved along with tracking the melt-solid interface. Therefore, eqn 14 for $0 \le i < i_b$, and eqn 15 and eqn 16 for $i = i_b$ are simultaneously integrated using a fourth-order Runge-Kutta algorithm, thus determining the temperature profile $T_i(t)$ and the location of the solid-melt interface $p(t)$.

B.3 Simulation parameters

An initial condition of $T_i = T_m$ is specified at all grid points. Either a constant temperature $T = T_l$ or a Neumann boundary condition $dT/dz = 0$ is imposed on the left hand boundary, $z = z_l$. Eqn 14 for $0 \le i < i_b$, and eqn 15 and eqn 16 for $i = i_b$ are simultaneously integrated using a fourth-order Runge-Kutta algorithm, thus determining the temperature profile $T_i(t)$ and the location of the solid-melt interface $p(t)$. In the results presented here, arbitrary scales are chosen to non-dimensionalise length z, time t and temperature T so that the dimensionless spatial and time domains span $\sim O(10^2)$ while the dimensionless temperature is $\sim O(1)$. Selecting the scaled values for $k/\rho C = 0.001$ and $\frac{L}{CT_0} = 0.001$ computations have been performed. A grid size $\Delta z = 0.1$ is chosen for discretizing the spatial domain. Similarly $\Delta t = 0.01$ is chosen as the time step for integration in order to accurately capture the progress of the interface between the grid points i_b and $i_b + 1$.

B.4 Results from the numerical simulations

A moving heat sink of velocity $v = 0.0009$ and strength $\dot{q} = 0.003$ is introduced at the left boundary at $t = 0$. Two different subcases are considered. In the first case, a constant temperature $T_l = -1$ is imposed on the left boundary of the domain. In the second case, the constant tempera-

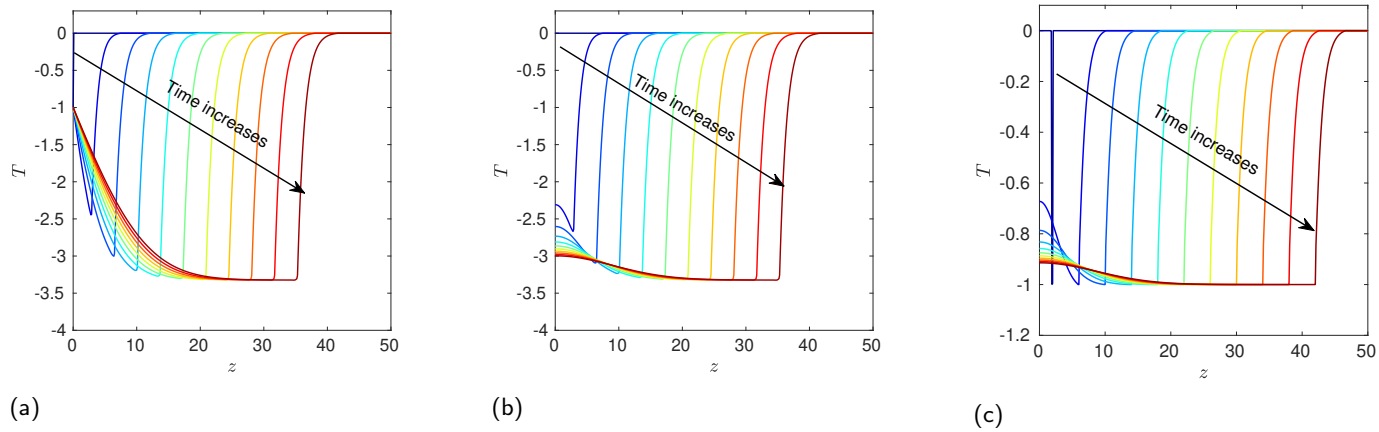

Fig. 5 Evolution of the temperature profile in the solid and the melt phase when a heat sink of strength $\dot{q} = 0.003$ is moved rightwards with a uniform velocity $v = 0.0009$, as time increases from $t = 0$ to $t = 40000$ (a) applying a constant temperature T_l on the left boundary, (b) applying Neumann boundary condition on the left boundary, and (c) replacing the moving heat sink of strength $\dot{q}$ with a moving constant temperature sink.

ture boundary condition is replaced by a no heat flux condition, $dT/dz = 0$, at the same boundary. The spatio-temporal evolution of the temperature profiles corresponding to these two cases are shown in Fig. 5a and Fig. 5b, respectively. In the former case, the temperature profile at $t = 0$ is a step function. The melt begins to crystallise as it loses heat to the two sinks, namely the left boundary (as in the Stefan problem) and the moving heat sink. The crystallising front moves right while the temperature in the solid continues to drop. Fig. 5a shows that a constant temperature, T_c, prevails in most of the solid region. Near the left boundary, there is a gradual change in temperature from T_l to T_c. On the right side of the constant temperature profile, a sharp variation in temperature is observed with temperature increasing from T_c to T_m. This change from a constant to a varying temperature occurs at the location of the moving heat sink, reminiscent of the analytical model described above. This temperature profile continuously translates rightwards as the heat sink and the crystallising front move.

A similar transient dynamics is observed in the second case (Fig. 5b) as well except with the difference that the left boundary does not contribute to cooling the system. The heat sink, initially located at $z = z_l = 0$ and moving with velocity v, removes heat from the system and the melt crystallises, creating a melt-solid interface. As the heat sink moves to the right, the interface also proceeds to the right. Meanwhile, the temperature in the solid continues to drop and approaches a constant temperature T_c, which is the same as that observed in the previous case. Similarly, the temperature of the crystallised solid to the right of the sink varies between T_c and T_m, as in the previous case.

In order to understand the generality of the resulting temperature profile due to a moving heat sink, we also carried out simulations by replacing the constant heat flux sink with a constant temperature sink located at $z_s(t)$. In the simulations, $T_s = -1$ and Neumann boundary conditions on the left boundary are used. As shown in Fig. 5c, the evolution of temperature profile is similar to the previous two cases, with a constant temperature to the left of the sink and a sharp increase from $T_c = T_s$ to T_m to the right of the sink are being observed.

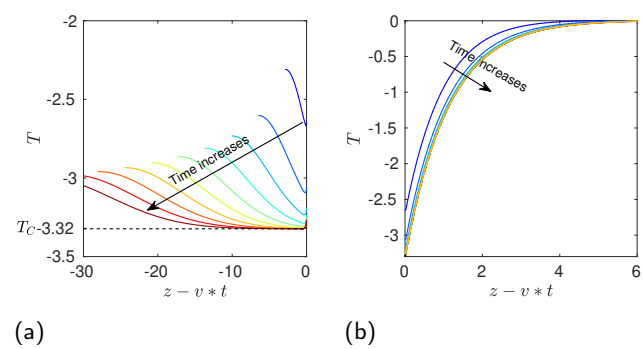

Fig. 6 The temperature profile in Fig. 5b in the crystallising solid at different instances of time mapped to a co-moving frame (a) on the left of the sink, $z_l < z < z_s$, and (b) in the sandwiched layer between the heat sink and the interface $z_s < z < z_0$. The dashed lines in both figures are the corresponding analytical solutions, eqn 12a and eqn 12b.

B.5 Transition from a self similar profile to a steady state solution

The spatio-temporal evolution of temperature in the material can be further analyzed by changing from a stationary to

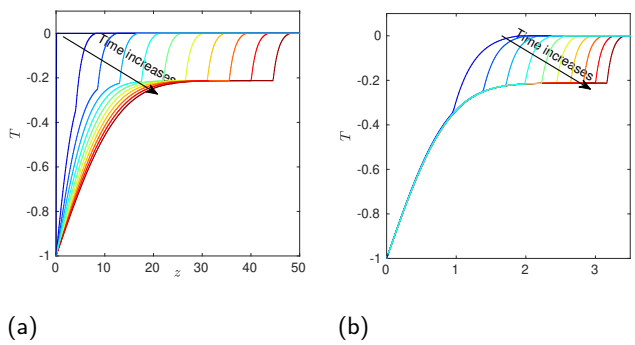

Fig. 7 Illustrating the transformation from the self-similar temperature profile (observed at initial times, $t << \alpha/v^2$) to a piecewise temperature profile (observed at long times, $t >> \alpha/v^2$) when the solid-melt interface is driven by a moving heat sink. (a) The spatio-temporal evolution $T(z,t)$, (b) temperature profiles in the similarity variable, $T(\eta)$. This analysis is done for the simulations where a constant temperature $T_l = 1$ is imposed on the left-hand boundary of the domain and a heat source of strength $\dot{q} = 0.0009$ moving rightwards with velocity $v = 0.0002$ is initially placed on the left boundary.

a reference frame translating with the heat sink. Since the temperature evolution in the three cases considered above were similar, we only analyze the second case further. The temperature profiles of Fig. 5b mapped into the moving frame are shown in Fig. 6. In order to understand the heat transfer process, we have further split the mapped temperature profiles in the solid region into two parts: (i) the region between the left boundary and the sink location, $z_l \leq z < z_s$, as shown in Fig. 6a and (ii) the region between the sink and the solid-melt interface, $z_s < z \leq z_0$, as shown in Fig. 6b. In Region 1, the temperature in the solid approaches a constant, and the length over which the plateau persists increases with time. On the other hand, Fig. 6b shows that the sandwiched layer between the sink and the interface has an exponential profile with the temperature increasing from T_c to T_m. Moreover, this exponential temperature distribution is invariant in time at long times. The analytical expressions for the steady-state temperature profile eqn 12a and eqn 12b are plotted as dashed lines in Fig. 6a and Fig. 6b, respectively, along with the temperature profile obtained from simulations. Clearly, there is a good match between the analytical and steady-state numerical solutions.

This transition from a self-similar to a piecewise profile can also be observed by following the transient temperature profiles as illustrated in Fig. 7. This analysis is done for the simulations shown in Fig. 5a where a constant temperature $T_l = -1$ is imposed on the left-hand boundary of the domain (as in the Stefan problem) and a moving heat sink of strength $\dot{q} = 0.0009$ and velocity $v = 0.0002$ is initially placed on the left boundary. Fig. 7a shows the evolution of the temperature profile in the solid phase. At $t = 0$, there is a step change in temperature at $z = 0$. As time proceeds, the classical Stefan temperature profile (described by eqn 10) emerges. This behaviour can also be inferred from Fig. 7b, where the temperature profiles follow the self-similarity variable at initial times. As time proceeds, the velocity of the interface continues to decrease and approaches the velocity of the moving sink (inherent velocity is comparable to the imposed velocity). Then, the system is no longer driven by the imposed temperature on the left boundary (Stefan problem), but rather by the moving heat sink, and the temperature profile switches over to the piecewise profile as shown in Fig. 7a.

The transition and attainment of a steady state solution can also be understood in terms of the velocity of the solid-melt interface. Initially, at $t = 0$, both the sink and the solid-melt interface are located at the left boundary. Therefore $z_0 - z_s = 0$ at $t = 0$. Soon crystallisation begins and the interface moves rightwards. The large interface velocity ($\sim 1/\sqrt{t}$) at small times leads the interface to drift away from the left boundary faster than the heat sink which moves with a constant velocity. Thus the distance between them increases. However, the interface velocity continuously decreases with time. Finally, when the interface velocity becomes equal to the velocity of the moving heat sink, the interface follows the moving heat sink. In other words, the solid-melt interface loses its natural velocity and the moving heat sink continuously propels the solid-melt interface. This zero relative velocity between the interface and the moving heat sink results in a constant separation between the two moving entities and so a steady state emerges. It may be noted that the steady-state velocity of the interface is exactly equal to the velocity of the heat sink irrespective of the strength of the heat sink; however, the separation distance $z_0 - z_s$ increases with increase in $\dot{q}$.

B.6 Effect of strength and velocity of the heat sink

While we have made qualitative comparisons between the simulations and the analytical predictions to this point, here we focus specifically on making quantitative comparisons. Fig. 8a shows the instantaneous temperature profiles when the strength of the heat sink is varied. For the case $\dot{q} = 0$, the melt does not crystallise and the material stays at the uniform temperature T_m. When $\dot{q} \neq 0$, the melt crystallises, and the temperature of the solid decreases and attains a plateau to the left of the heat sink. It is evident that the plateau temperature T_c decreases with $\dot{q}$ due to the availability of the large heat flux. A similar analysis is done when the velocity of the heat sink is varied but by keeping the strength of the heat sink constant. The crystallised solid to the left of the

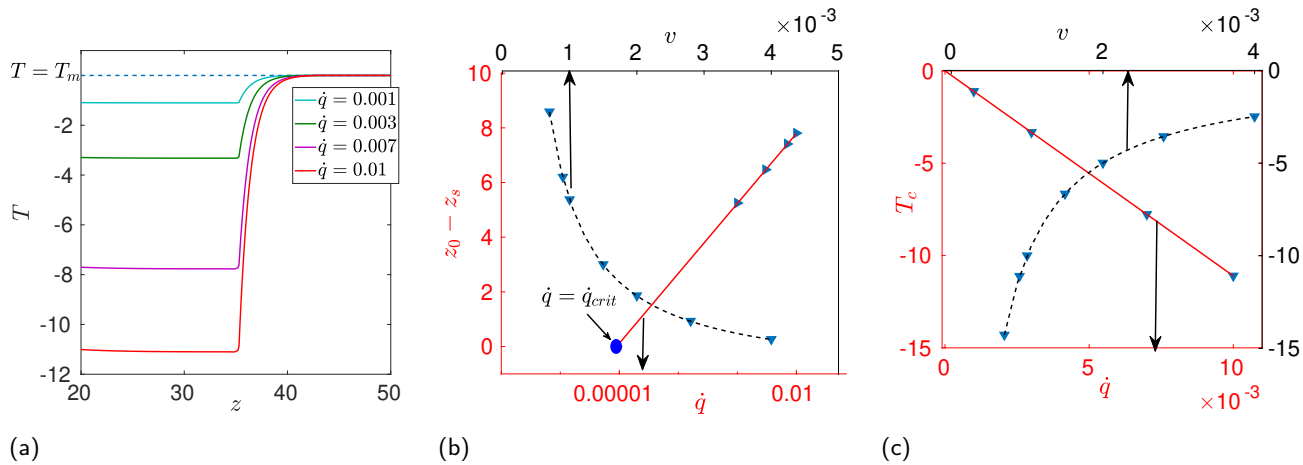

Fig. 8 (a) Temperature profiles at time $t = 40000$ for different $\dot{q}$ but at a fixed velocity $v = 0.0009$. (b) Steady-state separation distance between the heat sink and the solid-melt interface and (c) the plateau temperature T_c as a function of $\dot{q}$ (primary x-axis) and v (secondary x-axis). The dashed lines correspond to analytical solution, and the symbols are results from simulations.

sink attains a plateau temperature, T_c, irrespective of the velocity imposed, and this plateau temperature decreases with decreasing velocity of the heat sink. This occurs as more material is crystallised with increasing velocity of the heat sink, and thus less heat is available to reduce the temperature of the solid. In all cases, the temperature profile to the right of the sink is an exponential function as described by eqn 12b.

Fig. 8b shows the separation distance between the heat sink and the solid-melt interface, $z_0 - z_s$, as a function of the strength of the heat sink as well as its velocity. The results from the analytical calculations (eqn 13) and those from simulations are presented. Excellent agreement between the two approaches can be seen. It is also clear that the separation distance depends logarithmically on $\dot{q}$ and decreases with an increase in v. A similar plot for the plateau temperature T_c is shown in Fig. 8c as a function of the strength of the heat sink and its velocity. A good match between the analytical results (eqn 12a) and numerical simulations can be observed. Moreover, it can be seen that T_c varies linearly with $\dot{q}/v$.

B.7 Critical heat flux

Analysis of eqn 12a shows that if $|\dot{q}| < \rho v |L|$, then $T_c > T_m$, implying that the material to the left of the sink heats above its melting point. The specific heat required for this heating is taken away from the crystallising melt, and this situation is a clear violation of the second law of thermodynamics. In other words, there exists a critical heat flux $\dot{q}_{crit} = \rho v L$ beyond which only the steady state prevails.

B.8 Conclusions

We have analyzed the classical Stefan problem when augmented by a moving heat sink. In the absence of the moving heat sink, the Stefan problem does not have a steady-state solution. Instead, it develops a similarity form for the temperature profile. This is a consequence of the absence of any imposed length or velocity scales in the problem. The solid-melt interface moves diffusively ($\sim \sqrt{t}$) with an ever-reducing velocity.

When the phase change is induced by a moving heat sink, the system characteristics change. The imposed velocity of the sink drives the solid-melt interface to move with the same velocity. The resulting separation distance between the heat sink and the solid-melt interface represents a balance of diffusive and advective heat transfer processes. Thus, the system reaches a steady-state solution, with a constant temperature T_c to the left of the heat sink and an exponential variation from T_c to T_m for the sandwiched layer between the sink and the solid-melt interface. Here T_m is the melting point temperature of the solid. The similarity profile of temperature, a characteristic of the Stefan problem, is no longer relevant. The translating solid-melt interface switches over from a diffusive scaling $\sim \sqrt{t}$ (in the absence of a moving heat sink) to a ballistic scaling $\sim t$ (in presence of a moving heat sink). In this non-equilibrium but steady state, there is a continuous energy flux from the material to the moving heat sink.

These conclusions were reached both by numerical and analytical calculations independently. While numerical solutions provide insights into both transient and steady-state solutions, analytical calculations were restricted to only the latter state. However, the analytical calculations revealed the functional forms that describe the dependence of temperature profiles and the sink-interface separation distance on the strength and velocity of the heat sink. Moreover, analytical calculations showed that a steady-state solution with

a moving heat sink exists only if the heat flux to the sink is larger than a critical heat flux, $\dot{q}_{crit}$. Below this critical value, the melt will only be partially crystallised. This case of partial crystallisation, which arises in polymeric melts where the extent of crystallisation depends upon the degree of supercooling that the system is subjected to, is dealt in the main manuscript by incorporating Avrami kinetics into the heat balance.